Eddy Resolution versus Eddy Diffusion in a Double Gyre GCM. Part I: The Lagrangian and Eulerian Description

HORACIO A. FIGUEROA* AND DONALD B. OLSON

Rosenstiel School of Marine and Atmospheric Science, Division of Meteorology and Physical Oceanography, University of Miami, Coral Gables, Florida

(Manuscript received 26 May 1992, in final form 27 May 1993)

ABSTRACT

The Lagrangian and Eulerian descriptions of the flow in a double gyre, eddy-resolving numerical simulation are compared in the context of exploring the use of drifter arrays to describe ocean circulation. The parameterization of the unresolved scales of motion in large-scale numerical ocean models is analyzed through a combination of Lagrangian and Eulerian simulated fields. Here, in Part I, the Lagrangian and Eulerian description of the flow is presented with special emphasis on the description of the eddy diffusivity field. In Part II, the limitations that coarse spatial resolution imposes on the advective–diffusive equation are tested by comparing the evolution of a passive tracer field in high- and low-resolution numerical models.

The number of "buoy days" used in the numerical experiment is similar to what is expected to be launched in the Atlantic Ocean during WOCE/TOGA surface velocity program. The parameters that determine the model ocean circulation were chosen such that the mean and eddy kinetic energy levels are comparable to observations in the upper ocean. The diffusivity fields presented here are obtained from two different statistical approaches, namely, from the shear of the velocity field and from the application of Taylor's Lagrangian diffusion theory. This theory relates the absolute dispersion of tagged particles to the diffusive power of the turbulent velocity field in statistically homogeneous and stationary turbulent flows. By using a combination of Lagrangian and Eulerian statistics, it is observed that with a large number of particles the mean Eulerian velocities and velocity variances can be estimated well from the Lagrangian trajectories. The estimation of Lagrangian statistics (i.e., dispersion rates with respect to the center of mass, Taylor diffusivities, etc.) depends significantly on the region in which they are computed. The estimation of the spatial distribution of the diffusivity function from the trajectories of the particles released in the eddy-resolving numerical model reproduce the most important large-scale characteristics observed in the analysis of drifters and floats in the ocean: anisotropy of the horizontal components of the diffusivity matrix with zonal values usually being larger than meridional diffusivities, and an inhomogeneous diffusivity field, with large values in those regions where the eddy kinetic energy is larger. Central gyre statistics are typically well defined both in terms of the theory and within the drifter densities used. In the western boundary layer Lagrangian statistics are not robust, not because of sample size problems but due to the breakdown of the assumptions behind single particle calculations. Regimes where this occurs have ratios of the local advective time scale to the Lagrangian decorrelation time scale greater than one and are therefore typically nonstationary.

1. Introduction

One approach frequently used to describe tracer transport, both in oceanography and meteorology, is the analysis of the trajectories of fluid parcels. Because the conservation of properties is a Lagrangian concept, the use of Lagrangian current followers is a natural way to observe the horizontal (or quasi-horizontal) eddy processes and provide a description of lateral advection and eddy dispersion of the particles by the flow field. Particle trajectories and transport effects associated with different isolated features have been widely analyzed with both observations and numerical and analytical models. The Lagrangian approach to explore the ocean circulation is usually focused on the analysis of individual particles trajectories for different flow regimes and the use of Lagrangian statistics to describe the eddy transport.

As suggested in the pioneering work of Taylor (1921), Lagrangian statistics prove to be a useful tool to describe eddy transport. Taylor's work is considered to be the starting point of the classical diffusion theory. Its main contribution is to provide a way to estimate the diffusive power of a turbulent velocity field by analyzing the autocorrelation function of the Lagrangian velocity field. A large amount of research has been done using this approach both in the atmosphere and the ocean under the assumption that the Lagrangian sta-

* Current affiliation: Atmospheric and Oceanic Science Program, Princeton University, Princeton, New Jersey.

Corresponding author address: Dr. Horacio A. Figueroa, Atmospheric and Oceanic Sciences Program, Princeton University, Sayre Hall, P.O. Box CN710, Princeton, NJ 08544.

tistical analysis of atmospheric balloons (Kao 1965) and floats, respectively, provides a measure of the diffusivity field (Freeland et al. 1975; Davis 1985; Colin de Verdiere 1983; Krauss and Böning 1987; Figueroa and Olson 1989). This analysis has also extended to basin-scale eddy resolving numerical models (Böning and Cox 1988).

Böning and Cox (1988) were the first to examine the eddy diffusive properties of a flow field in a basin-scale eddy resolving primitive equation numerical model of the ocean circulation by using Lagrangian trajectory simulations. Their analysis is limited to the relatively homogeneous eastern part of the interior of the subtropical thermocline where the concept of eddy diffusivity is more likely to apply because of the homogeneity of the velocity field. By using interpolated data archived every 3 days, they estimate eddy diffusivities in the model thermocline to be on the order of 5×10^7 cm^2 s^{-1}. This value is a factor of 3 larger than oceanic observations for these areas. Their analysis, however, is restricted to the gyre interior, and no diffusivity estimations are presented for the western boundary and the high eddy kinetic energy regions.

The novel approach of this work is that it goes one step further in relating the Lagrangian and Eulerian approaches in describing the mixing of passive tracers. This is done by looking at how well the dispersion of drifters, and the eddy diffusive properties of the mesoscale eddy field inferred from them, represent the actual diffusion and mixing of tracers.

The goals of Part I are therefore to investigate the feasibility of estimating relatively accurate eddy diffusion coefficients and other low-order Lagrangian statistics from the trajectories of numerical particles released in an eddy-resolving numerical model of the ocean circulation. Thus, the Lagrangian and Eulerian description of the flow is presented with particular emphasis on the estimation of the dispersive properties of the eddy velocity field. In Part II, we make use of these Lagrangian statistics to analyze the evolution of passive tracer fields. Here it is assumed that the classical diffusion theory of Taylor (1921), based on the statistical analysis of the dispersion of single particles in stationary and homogeneous flows, is capable of describing the diffusive power of the eddy velocity fields.

The layout of this work is as follows. In section 2, the Bleck and Boudra (1986) numerical model equations and characteristics are briefly reviewed. In section 3, the numerical techniques associated with the tracking of Lagrangian particles in Eulerian numerical models are discussed. In section 4, the results from the eddy resolving experiments are presented. The discussion is based on the analysis of the Lagrangian and Eulerian statistics computed from the numerical model. These statistics are the spatial distributions of diffusivity functions, Lagrangian integral time scale, kinetic energies, and dispersion rates. A discussion of the results as well as their significance to the execution of field programs and modeling of passive tracers is presented in section 5.

2. Description of the model

The original code first developed by Bleck and Boudra (1981) for a hybrid vertical coordinate system, and later implemented to pure isopycnic coordinates (Bleck and Boudra 1986), had been used extensively for exploring the wind-driven circulation on basin scales for both coarse- and high-resolution simulations (Boudra and Chassignet 1988; Campos and Olson 1991; among others). Here, the Bleck and Boudra (1986) isopycnal coordinate primitive equation model is used. The equations of motion for each layer are basically the shallow-water equations, and there is no fluid motion across the coordinate surfaces. Layers interact only through hydrostatically transmitted pressure forces. The layer-integrated horizontal momentum equations in generalized coordinates with s as the vertical coordinate are according to Bleck (1979):

$$\frac{\partial \mathbf{V}}{\partial t} = -\frac{1}{2}\cdot\nabla_s\mathbf{V}^2 - (\zeta_s + f)\mathbf{k}\times\mathbf{V} - \left(\dot{s}\frac{\partial p}{\partial s}\right)\frac{\partial \mathbf{V}}{\partial s} - \alpha\nabla_s p - \nabla_s\phi + \alpha\frac{\partial \tau}{\partial z} + A\left(\frac{\partial p}{\partial s}\right)^{-1}\nabla_s\cdot\left(\frac{\partial p}{\partial s}\nabla_s\mathbf{V}\right), \quad (1)$$

where

$$\zeta_s = \frac{\partial v}{\partial x} - \frac{\partial u}{\partial y}$$

is the relative vorticity on s, α is the specific volume within the layer, $\dot{s} = ds/dt$, ϕ is the geopotential, and A is the eddy viscosity coefficient. Other symbols are conventional.

The continuity equation in isopycnal coordinates, which does not include any thickness diffusion term, is given by

$$\frac{d\Delta p}{dt} = 0, \quad (2)$$

where Δp is the layer thickness. The hydrostatic equation is given by

$$\delta M = p\delta\alpha. \quad (3)$$

The horizontal pressure force is expressed in terms of both geopotential and pressure gradients along coordinate surfaces represented by the Montgomery potential ($M = gz + p\alpha$). Since there are no diabatic processes or compressibility effects considered, there is no thermodynamic equation to be solved. The numerical techniques used in the model integration are presented in Bleck and Boudra (1986) and, therefore, are not discussed here.

Parameter setting

The parameters that determine the model ocean circulation were chosen such that the eddy kinetic energy levels are comparable to observations (Richardson 1983; Piola et al. 1987) in the upper ocean (Fig. 1a).

Depth	$H = 4000$ m
Upper-layer thickness	$h_1 = 500$ m
Lower-layer thickness	$h_2 = 3500$ m
Reduced gravity	$g' = 0.02$ m s^{-2}
Wind stress amplitude	$\tau_0 = 0.1$ N m^{-2}
Viscosity	$A = 50$ m^2 s^{-1}
Coriolis parameter	$f_0 = 8.3 \cdot 10^{-5}$ s^{-1}
Meridional coriolis variation	$\beta = 2.0 \cdot 10^{-11}$ m^{-1} s^{-1}
Bottom friction	$\epsilon = 1.0 \cdot 10^{-7}$ s^{-1}
Horizontal resolution	$\Delta x = 20$ km

The boundary conditions are given by

$$u = \frac{\partial v}{\partial x} = 0 \quad \text{at} \quad x = 0, L_x;$$

$$v = \frac{\partial u}{\partial y} = 0 \quad \text{at} \quad y = 0, L_y,$$

which correspond to free slip lateral boundary condition. The implementation of free slip boundary conditions for the C grid used here is discussed in Campos (1990). The ocean is driven by a zonal wind stress (τ_x, 0), given by $\tau_x = -\tau_0 \cos(2\pi y/L_y)$, where L_y is the meridional extent of the basin. No buoyancy forcing, besides the one on the form of pressure forces between the layers, is included. For the parameter setting as described above, the observed scales for the isopycnal velocity, (U), horizontal scale (L), and vertical scale (D), are 30 cm s^{-1}, 100 km, and 500 m, respectively. The associated Rossby radius of deformation is about 40 km, and the Reynolds and Burger numbers are of the order of 600 and 0.1, respectively. The high Reynolds number clearly indicates the turbulent characteristics of the model simulations, while the Burger number provides a measure of the ratio of the radius of deformation to the typical length scale.

Results from wind-driven primitive equation models in a double gyre configuration with square geometry and flat bottom are extensively discussed in the literature (Holland and Lin 1975; Holland 1978; Bleck and Boudra 1981, 1986; Huang 1986; and others). Therefore, the discussion here will only briefly treat aspects of the circulation that are considered in the aforementioned papers and will focus on mixing in this well-studied configuration.

Figure 1a shows the eddy kinetic energy field and Fig. 1b shows a series of instantaneous maps of the upper-layer circulation represented by the layer thickness field. The circulation in this layer is composed of a subtropical and subpolar gyre with an eastward flowing free jet in between. The high Reynolds number characterizing the circulation, together with the high resolution (Δx, Δy = 20 km) and relatively low ratio of the upper to lower layer depth ($H_1/H_2 = 0.14$) results in a circulation that is very nonlinear and in which eddies form almost continuously over most of the basin. Figure 2 depicts the mean circulation for the same layer, averaged over the last 4000 days (~11 years) of the model integration.

3. Lagrangian statistics

Figures 3 and 4 show[1] the spaghetti plots corresponding to two sets of Lagrangian trajectories launched in Northern Hemisphere subtropical and subpolar gyres, respectively. The particles launched in the subtropical gyre (Fig. 3) exhibit more turbulent trajectories as they drift westward than those moving in the same direction and launched in the subpolar gyre (Fig. 4). This behavior is consistent with the smaller upper-layer depth in the northern part of the basin (than in the southern), which results in a more nonlinear regime. Eddies, characterized by closed particle trajectories, are observed to exist almost everywhere in the basin.

Bower (1991) studied the mechanisms by which fluid particles cross a meandering jet. Her results suggest that the ability of particles to cross the meandering jet stream is determined to a large extent by the motion of the water parcel along the stream relative to the meander propagation and by the initial position of the particles relative to the core of the stream. Recent observations in the Gulf Stream (Bower and Rossby 1989) reveal that only a small number of subsurface RAFOS floats actually travel across the stream. The particle trajectories presented here do not show evidence of this behavior, although they suggest that a small number of particles can be trapped in forming eddies and move across the gyre trapped in the eddy. Two likely explanations for this behavior can be put forward. As suggested by Owens (1984), if the alongstream velocity of the particles exceeds the typical phase speed of the propagating meander, fluid particles are likely to be trapped in the current. The second explanation is that the sharp meridional potential vorticity gradient observed in the region of the jet acts as barrier to the exchange of particles. It should be kept in mind that the Lagrangian particles are not affected by particle inertia and that because of the spatial resolution used here (20 km), the particle trajectories are not affected by smaller-scale phenomena.

[1] Here, only a small fraction of the total number of trajectories used in this study is presented.

The statistical background

Eulerian statistics from Lagrangian trajectories are estimated from a combination of spatial and temporal averaging. Lagrangian statistics, on the other hand, consider observations made following particles *launched* in a region. The requirement is usually relaxed by using all particles that pass through a region.

The computation of autocorrelation functions, diffusivity functions, and dispersion rates requires the separation of the instantaneous velocity into a mean component plus a fluctuation with respect to the mean. When only Lagrangian data is available, as is usually the case from observations in the real ocean, the mean velocities removed from the velocity time series are the ones obtained by averaging all existing estimates in a given region. Here, the availability of a mean velocity field estimated from both the Lagrangian trajectories and the Eulerian gridpoint values provides the means for comparing both fields (Figs. 5a,b).

The Lagrangian statistics discussed in this section were estimated from the trajectories obtained from 200 particles randomly deployed over the basin. The model ocean was integrated for a period of 4000 days ($\sim$11 years) after equilibrium, providing 8×10^5 buoy-days. The integration was carried out in four periods of 1000 days each. At the beginning of each period the Lagrangian particles were randomly seeded. This was done in order to reduce bias and maintain a relatively uniform float density distribution.

Eulerian averaging is used to estimate mean velocities and single particle diffusivity from the Lagrangian particles. As indicated by Davis (1983, 1985), there are three basic ways that Eulerian statistics derived from Lagrangian data can be biased. These are:

1) Bias originated by Stokes drift, which induces higher-order terms (i.e., $V_L = U_E + l'(\partial U_E/\partial x)$). These terms correspond to the Lagrangian mean velocity, the Eulerian mean, and the product of the Lagrangian displacement by the Eulerian velocity gradient, respectively. This suggests that if particles are not uniformly distributed, there is a difference between random deployment and random encounter statistics.

2) The existence of a correlation between launching position and the mean drift.

3) Inhomogeneities of the eddy velocity field, which cause particles to drift toward high eddy energy regions (Freeland et al. 1975).

The main features observed from the gridpoint velocities are well represented by the Lagrangian particles, although minor differences due to a lack of continuity of the Lagrangian sampling can be observed. The Eulerian mean velocity components obtained from the Lagrangian particles drift are estimated by partitioning the ocean basin into subblocks of 2 by 2 model grid elements and ensemble averaging float velocities over each subdomain area. In this way the Eulerian statistics

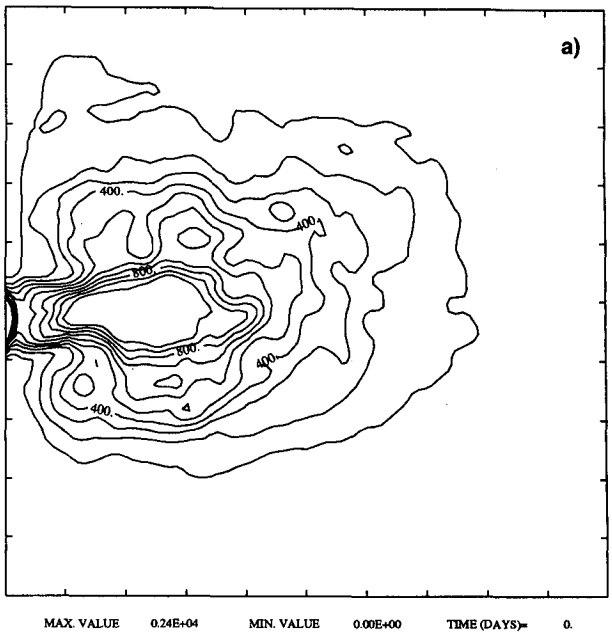

FIG. 1. (a) Eulerian eddy kinetic energy in cm^2 s^{-2}. (b) Instantaneous maps of the upper-layer circulation represented by the layer thickness. Maps are presented every 10 days.

from the floats are obtained for 40 km $\times$ 40 km areas. The 40 km $\times$ 40 km size of the subblocks is a compromise between spatial resolution, statistical stability, and representativeness. Figures 6a,b show the correlation between the mean velocity components as determined from the gridpoint values and from the Lagrangian trajectories. The influence of the westward propagation of the planetary waves on the float-derived mean velocity field is represented by the departure of the scatter points with respect to the diagonal solid line. Note that this departure is larger for the high zonal velocity estimates characteristic of the free jet. The correlation in the meridional component shows that the absolute value of the float-derived mean velocities is systematically larger than the mean Eulerian velocities, particularly in the western boundary layer, where velocities are higher. Probably, the 40 km $\times$ 40 km subblocks in the western boundary region for which the Lagrangian mean velocities are estimated is too wide to resolve the western boundary current, underestimating its value.

This averaging procedure of computing the arithmetic mean value from all observations in a bin is biased toward low velocity episodes, as water parcels trapped in slow moving features will remain longer in an area than those trapped in fast moving features. One alternative to reduce this source of bias is by considering only independent observations, by applying some combination of temporal and spatial filtering of the available data. This procedure is implemented here by assuming a decorrelation time scale of the order of

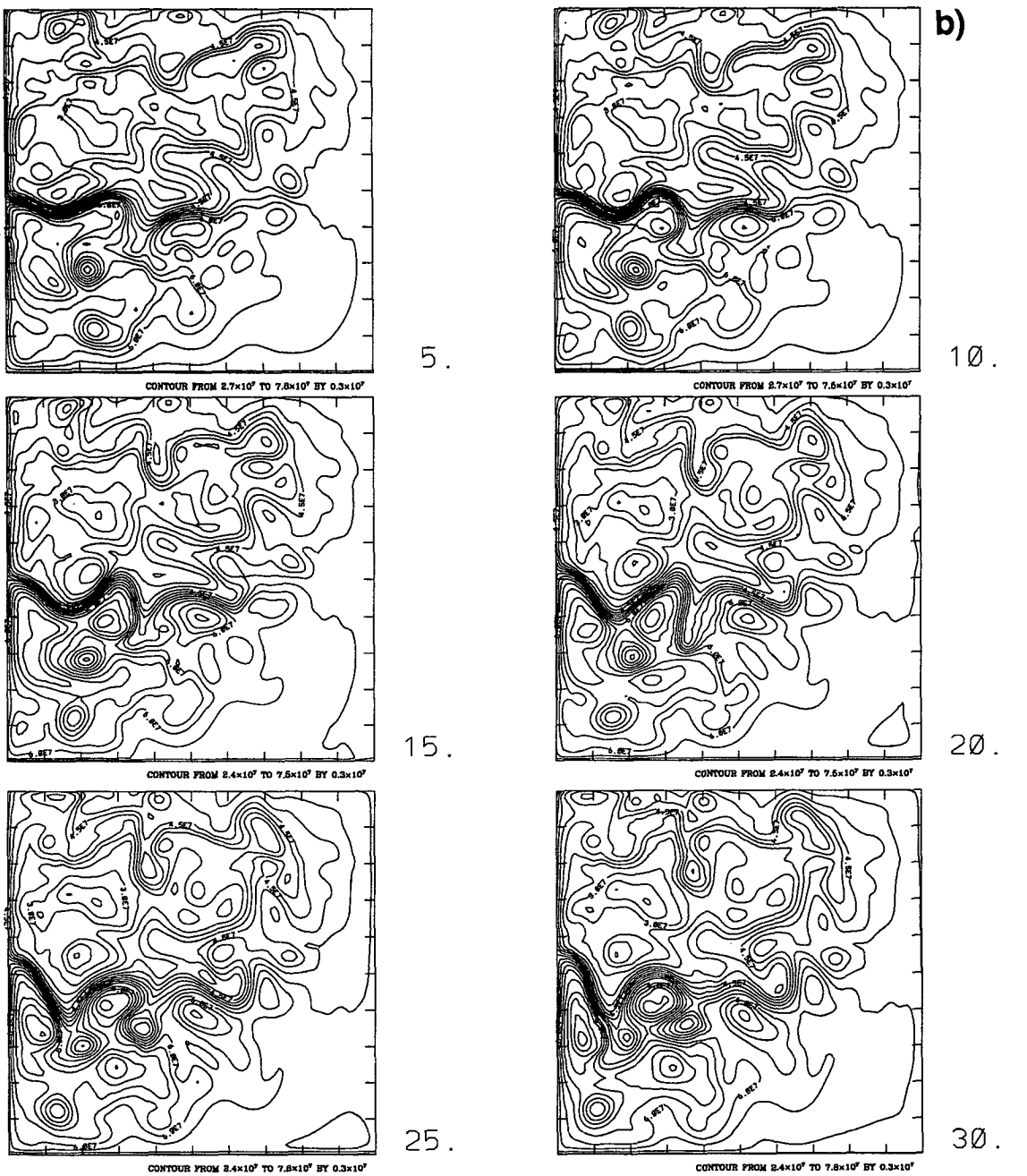

FIG. 1. (*Continued*)

5 days and thus using only independent velocities separated by a typical time scale. If, for example, two particles are in the same 40 km × 40 km bin within the temporal window of a typical Lagrangian integral time scale of 5 days, the velocities will not be independent of each other. In this case, the value corresponding to the velocity averaged over all the available data during that period (5 days) is used as an individual observation. The same averaging procedure is considered when a Lagrangian particle stays in the bin over a period shorter than the typical time scale. This method of computing Eulerian average velocities from Lagrangian data gives mean kinetic energy levels that are about 16% higher than those estimated by considering all available data inside the bin.

4. The diffusivity fields

The Eulerian and Lagrangian statistics to be discussed in what follows are meant to serve as a link

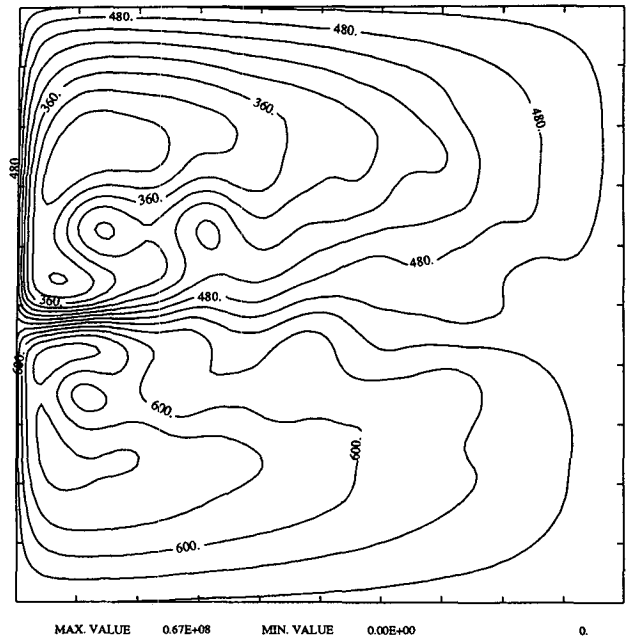

FIG. 2. Upper-layer mean circulation averaged over the last 4000 days (~11 years) of integration.

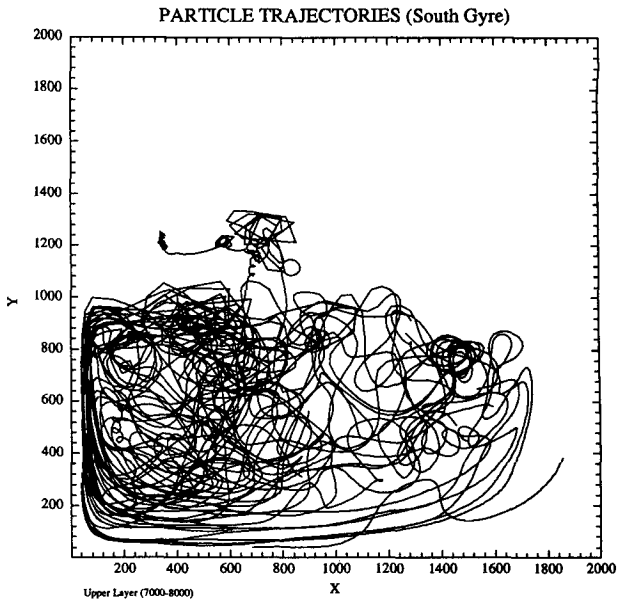

FIG. 3. Spaghetti diagram corresponding to a small fraction of the Lagrangian trajectories launched in the subtropical gyre. Axis is given in kilometers.

between Lagrangian particle motions, mixing length theories, and Lagrangian diffusion, and the use of the advection–diffusion equation for passive tracers (Part II) in which the eddy transport is governed by an eddy diffusivity, considered in the following section.

There are several approaches used to describe eddy transport in numerical models. The most widely used is Laplacian diffusion (the flux vs gradient law) in which the factor of proportionality is tuned to maintain numerical stability. Here, two approaches are examined. The first represents a Lagrangian view of the problem in which the dispersion of Lagrangian particles are used to compute the lateral components of the space-dependent diffusivity. The second is an Eulerian approach in which the mean shear of the instantaneous velocity field is used to estimate a deformation-dependent diffusion coefficient. The two diffusivity fields resulting from the Lagrangian and Eulerian approaches mentioned above are discussed here and are used in Part II to investigate the usefulness of a space-dependent and anisotropic diffusivity field in the integration of the advective–diffusive equation for a passive tracer field.

a. Lagrangian diffusivity

The statistical background supporting the computations presented in what follows is discussed in several papers (Freeland et al. 1975; Colin de Verdiere 1983; among others). These statistics are autocorrelation functions, diffusivity functions, dispersion rates, and Lagrangian integral time scales. The main restriction for the application of the classical diffusion theory of Taylor is the homogeneity and stationarity of the turbulent velocity field. These concepts are necessarily related to specific spatial and temporal scales. An ocean basin, for example, is certainly not homogeneous, and if the observations are taken over a period of a year, it is nonstationary as well. However, by reducing the spa-

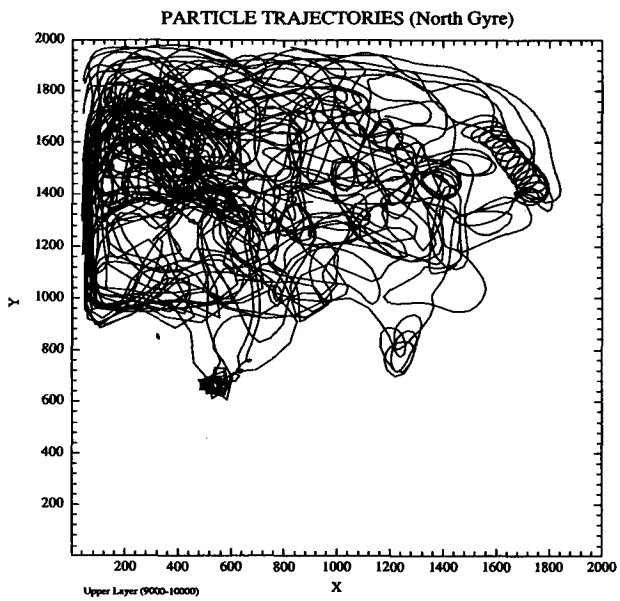

FIG. 4. Spaghetti diagram corresponding a small fraction of the Lagrangian trajectories launched in the subpolar gyre.

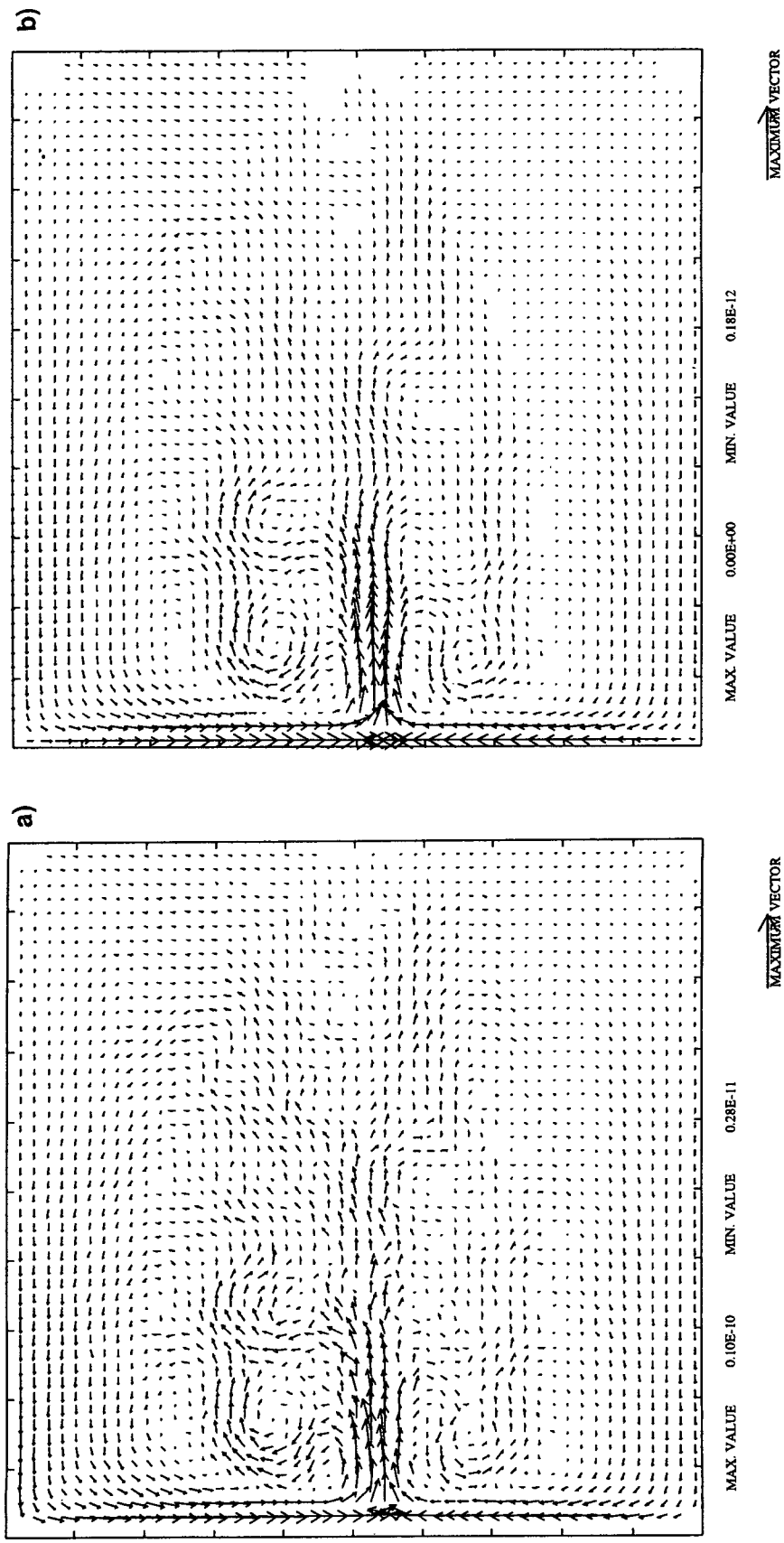

FIG. 5. (a) Mean velocity field as obtained from the Lagrangian particles and (b) from the Eulerian field. Arrows are plotted at alternate grid points. Maximum velocities are of the order of 60 cm s^{-1}.

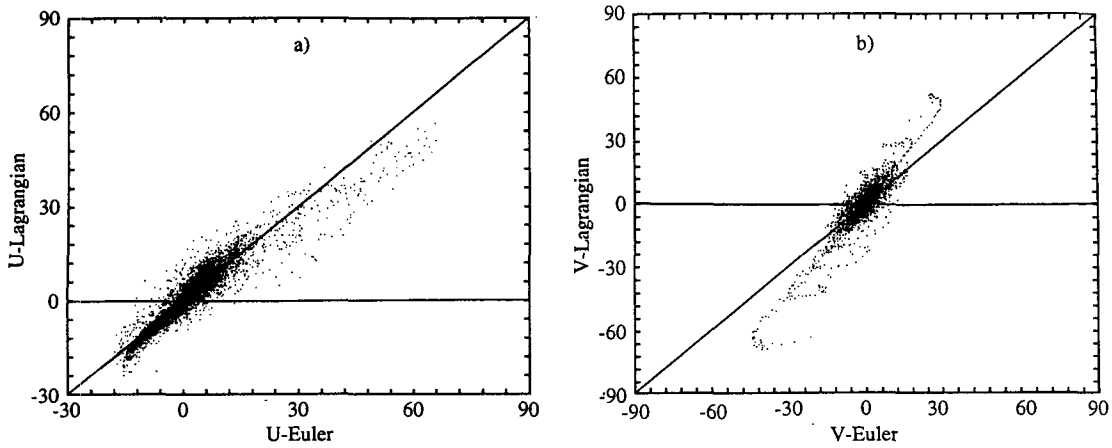

FIG. 6. Correlation between mean zonal (a) and meridional (b) velocity components as obtained from the Lagrangian particles and from the Eulerian field. Each dot corresponds to a gridpoint observation from the previous map. Velocities are given in centimeters per second.

tial scales over which statistics are estimated, the condition of homogeneity can be approximated. Analogously, if observations are taken over long periods so that the lower frequencies can be resolved, the associated statistics can be considered stationary. A third possibility is the existence of an energy gap between low-frequency fluctuations and the dominant frequencies in the signal. The application of the first of these restrictions to the estimation of Lagrangian diffusivities from the numerical model would impose severe constraints on the size of the bins, particularly near the western boundary. Reducing the size of the bins generates a problem with the resolution of the autocorrelation function. Thus, the size of the bins represents a compromise between resolution and representativity.

Of the several steps usually taken to go from the Lagrangian velocity time series obtained from drifting floats to the ensemble-averaged particle dispersion to be presented, there are three functional steps in which homogeneity and stationarity are explicitly assumed. The first of these three is to assume that the autocorrelation of the velocity field determines the joint probability distribution function; thus, the autocorrelation function can be used to describe the turbulent field. The second one, which is basically the definition of homogeneity, is that $\bar{u} \neq \bar{u}(x, y)$ and that $\overline{u'^2} \neq \overline{u'^2}(x, y)$. And the third one is to assume that the statistics are independent of the launching time and position.

The size of the bins used for the estimation of the autocorrelation functions, diffusivity functions, and dispersion rates from the Lagrangian trajectories is 200 km × 200 km. Each bin contains 10 model grid points in each direction. The number of floats passing through each bin over the duration of the experiment is about 100 ± 20, providing more than 5000 daily velocities per bin. Despite the large sampling array, not all Lagrangian time series are suitable to be used in the estimation of the autocorrelation function. In most bins, only a relatively small fraction (40% or less) of the total number of particles depicts an autocorrelation function with a zero crossing. This zero crossing is indicative of the existence of a high-frequency eddy field. The other 60% of the Lagrangian time series do not show a zero crossing. The spatial distribution of the autocorrelation function calculated from Eq. (4) is presented in Fig. 7. The autocorrelation function of the Lagrangian velocity field $[R_{ij}(\tau)]$ is given by

$$R_{ij}(\tau) = \frac{1}{\overline{u_i'^2}} \left\langle \frac{1}{T} \int_0^\infty u_i'(t) u_j'(t+\tau) dt \right\rangle, \quad (4)$$

where the primes denote the velocity fluctuations with respect to the Eulerian mean velocity, and i and j refer to the horizontal direction; τ is the time lag, and T is the maximum lag. Each small frame depicts the zonal (dashed line) and meridional (solid line) ensemble-averaged autocorrelation function corresponding to each 200 km × 200 km bin. The x axis in each frame corresponds to the time lag that goes from 0 to 30 days. (In some cases, the length of the function exceeds 30 days and extends into the neighboring frame.) The y axis corresponds to the value of the autocorrelation function, which can vary between −1 and 1. The decorrelation time is represented by the first zero crossing. Deep negative and positive oscillations in the autocorrelation function denote the existence of energetic coherent structures in the turbulent velocity field.

One of the major limitations of estimating diffusivities from the Lagrangian autocorrelation function is the resolution of the small-scale eddy velocity ($l < 200$ km) by individual particle trajectories. When the advective time scale, defined as the ratio of the size of the bin to the mean velocity, is smaller than the decorrelation time of the Lagrangian trajectory (i.e., $l/U_E < \tau_d$), the zero crossing of the autocorrelation

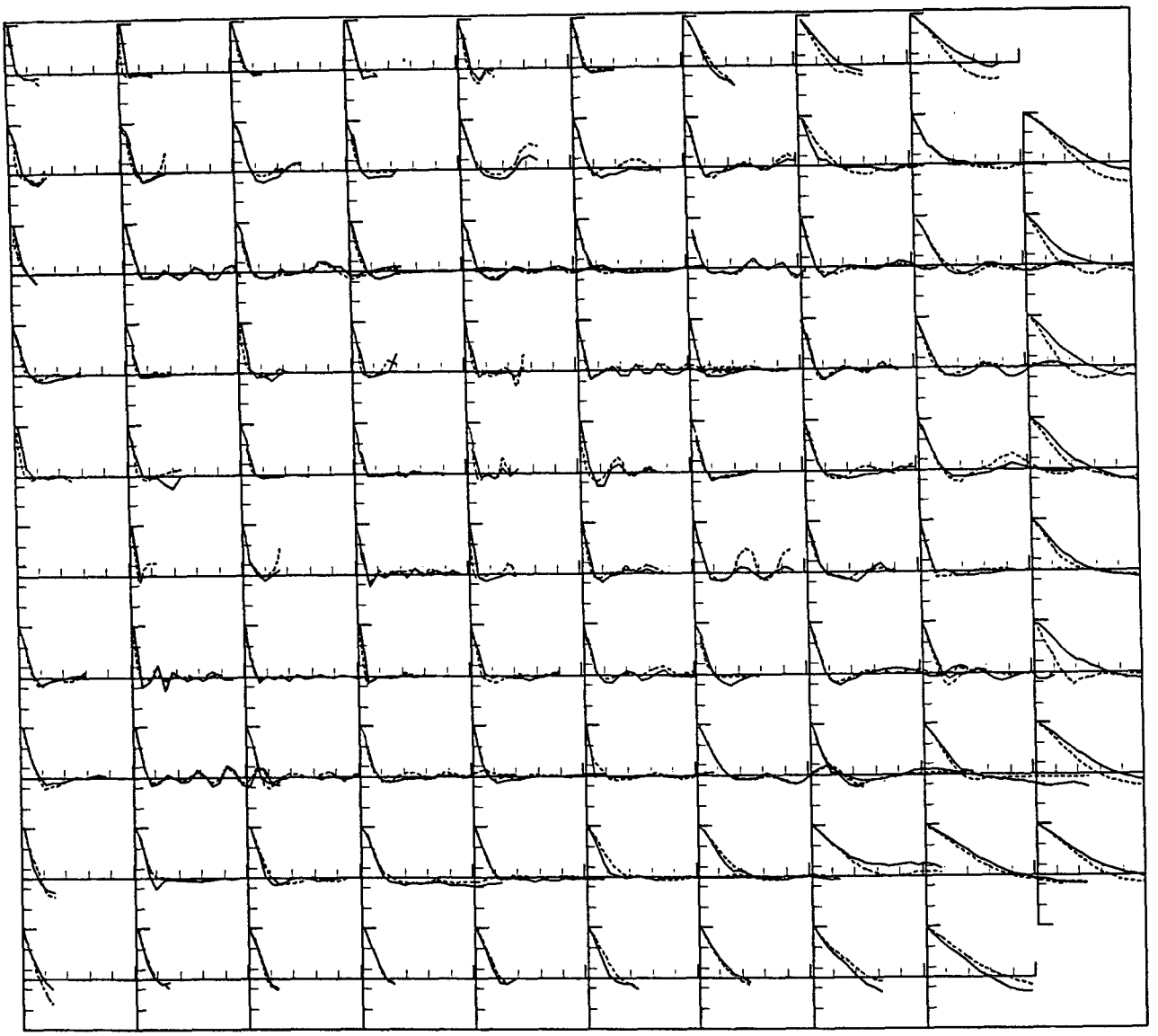

FIG. 7. Map of the autocorrelation function. Each small frame depicts the zonal (dashed line) and meridional (solid line) ensemble averaged autocorrelation function corresponding to each 200 km × 200 km bin. The x axis in each frame corresponds to a time lag that goes from 0 to 30 days. The y axis varies between −1 and 1.

function is not resolved. Thus, the diffusivity function does not reach an asymptotic value as required by definition. This problem, which is characteristic of high velocity regions like western boundary currents and their seaward extension is independent of the number of floats used and is intrinsic to the Lagrangian view of an inhomogeneous field and the computation of Eulerian statistics from Lagrangian velocities. The lack of resolution of the small-scale eddy signals by a particular float trajectory suggests that trajectory should not be used in the computations of the "bin-scale" (200 km) diffusivity function. This restriction significantly reduces the number of "adequate" trajectories used to estimate the autocorrelation and diffusivity ensemble averages in some regions. This troublesome characteristic of Lagrangian sampling is circumvented here by using only those trajectories whose velocity time series decorrelate while in the bin.

Figure 8 shows the spatial distribution of the diffusivity function $K_{ij}(t)$ estimated according to Eq. (5):

$$K_{ij}(t) = \overline{u_{ij}'^2} \int_0^t R_{ij}(\tau)d\tau. \qquad (5)$$

The limits of the y axis (Fig. 8) are different for each bin so that the diffusivity function in all bins can be

presented in the same map. Note that there can be a difference of up to two orders of magnitude between the diffusivity in the region of the free jet and in the interior. The typical diffusivity curve for homogeneous turbulence is characterized by a monotonic growth over a decorrelation time scale, followed by a plateau that represents the K^{∞} or diffusivity coefficient. Observations of the diffusivity function, both in these simulations (Fig. 8, Table 1) and from floats in the ocean (Freeland et al. 1975; Krauss and Böning 1988), rarely exhibit this theoretical plateau. In the bins in which the eddy velocity field consist of energetic coherent features, the diffusivity function shows some oscillations superimposed on a steady growth. In some cases, the diffusivity function shows a monotonic decrease after reaching a maximum value suggesting the existence of an unresolved low-frequency eddy field. The spatial distribution of the diffusivity curves presented here suggest that it is not very easy to characterize the curves according to the various regimes observed in the model ocean, namely, western boundary currents, recirculation regions, etc. Most diffusivity curves clearly show the existence of a strong coherent eddy field. In only a small number of bins is the asymptotic diffusivity (K^{∞}) actually reached. This suggests that integrating Eq. (5) over the length of the diffusivity series (T) results in a diffusivity coefficient that can be too dependent on the limits of integration. If, on the other

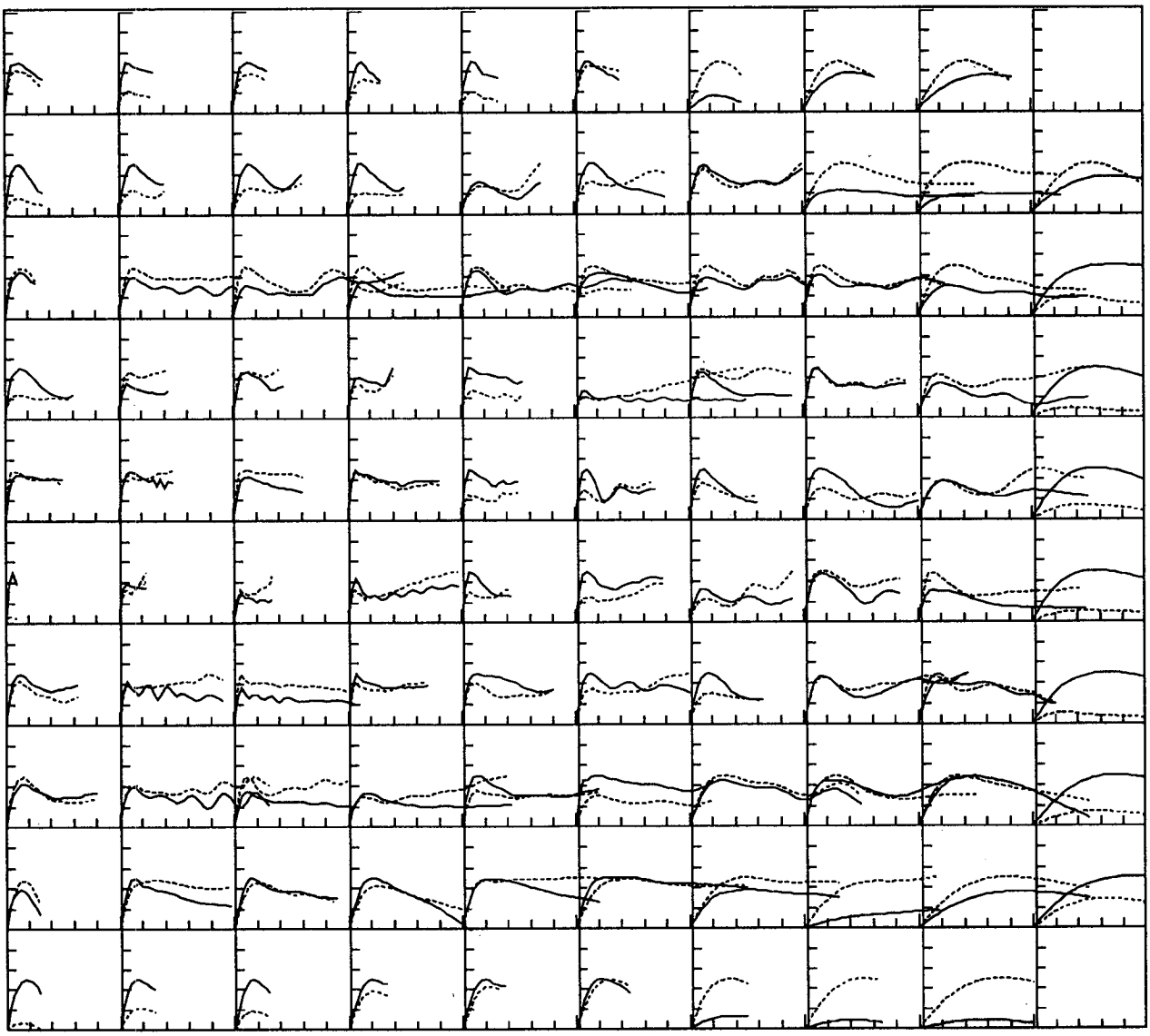

FIG. 8. Map of the diffusivity function. Each small frame depicts the zonal (dashed line) and meridional (solid line) ensemble-averaged diffusivity function corresponding to each 200 km × 200 km bin. The x axis in each frame corresponds to a time lag that goes from 0 to 30 days. The y axis varies from one frame to another.

TABLE 1. Approximate diffusivity values per region in 10^7 cm^2 s^{-1}.

Region	Lower-limit Lagrangian		Upper-limit Lagrangian		Deformation
	K_{xx}	K_{yy}	K_{xx}	K_{yy}	K_H
Subtropical gyre	0.9	0.8	0.9	0.8	0.7
Subpolar gyre	1.1	1.2	1.0	1.3	0.9
Western boundary current	2.1	2.0	3.8	3.9	5.3
Free jet	6.0	4.1	7.1	5.9	4.8

hand, the K^∞ is estimated by integrating this equation only up to the first zero crossing of the autocorrelation function, it will represent an upper limit to the "true" K^∞. The two estimations, however, might coincide in a few cases.

A second restriction in the estimation of the diffusivity coefficient from the integration of the autocorrelation function is based on the assumption that negative side lobes after a decorrelation time scale are not statistically significant. Thus, the integration in Eq. (5) is performed only up to the first zero crossing of the autocorrelation function. This assumption is considered by Krauss and Böning (1988). The justification for this is that, as shown by Davis (1991), for large t, the sampling error of $K(t)$ increases roughly as $t^{1/2}$ due to a reduction in the sample size. Thus, $K(t)$ is less accurate as t increases. By considering $K(t_0) \sim K^\infty$, where t_0 represents the time corresponding to the first zero crossing, it is assumed that K^∞ represents an upper limit to the diffusivity coefficient.

These ideas apply particularly to the interpretation of the evolution of tracer fields. Basically, they suggest that if the time scale over which $K(t)$ approaches K^∞ is short compared to the time scale over which the mean tracer field evolves, the classical eddy diffusion law, with the time-independent diffusivity K^∞, will approximate the elaborated advection–diffusion equation developed by Davis (1987), in which the diffusivity term considers a time-dependent diffusivity.

Based on the preceding considerations, the two methods of computing the diffusivity coefficient (integrating up to the first zero crossing and integrating over the length of the autocorrelation function) represent an upper and a lower diffusivity limit. In Fig. 9 the spatial distribution of the four elements of the isopycnal diffusivity matrix is presented (from the integration over the length of the series). Consistent with theory and observations, the maximum values are associated with the region of the free jet and decay eastward (Table 1). These characteristics are evident from studies in the region of the Brazil/Malvinas currents (Figueroa and Olson 1989). Particularly near the western boundary layer, the negative zonal gradient of the zonal diffusivity results in a negative zonal advective effect. This is represented by

$$\frac{\partial}{\partial x}\left(K_{xx}\frac{\partial \theta}{\partial x}\right) = \frac{\partial K_{xx}}{\partial x}\frac{\partial \theta}{\partial x} + K_{xx}\frac{\partial^2 \theta}{\partial x^2}.$$

Therefore, the space-dependent diffusivity near the western boundary layer has the opposing effects of generating an eastward diffusion due to the tracer gradient and a westward advective effect due to the diffusivity gradient.

The ocean interior (Fig. 9) shows a diffusivity distribution that is about two orders of magnitude smaller than in the region of the jet. This is consistent with the eddy kinetic energy distributions. The off-diagonal elements of the diffusivity matrix have both positive and negative values that are of the same order of magnitude as the diagonal elements. This suggests that neglecting these terms in the advective–diffusive equation can misrepresent the diffusive power of the eddies. It also implies an active interaction between waves and the mean flow that exceeds the familiar Fickian formulation with a constant diffusivity. The diffusivity distribution presented here shows some of the characteristics observed in Figueroa and Olson (1989) from the Southern Ocean studies and the First GARP (Global Atmospheric Research Program) Global Experiment surface drifters, namely, a highly inhomogeneous spatial distribution, horizontal anisotropy with zonal values being large than meridional, away from the western boundary layers, and a fair correlation eddy velocity field.

Taylor's (1921) theory states that in homogeneous and stationary turbulent flows the rate of dispersion of Lagrangian particles is related to the autocorrelation function by

$$\overline{X'^2_{ij}}(t) = 2\overline{u'^2_{ij}}\int_0^T \int_0^t R_{ij}(\tau)\,d\tau dt, \qquad (6)$$

where i and j correspond to the zonal and meridional components, $\overline{X'^2_{ij}}(t)$ is the variance of the eddy displacement, and u'^2 is the velocity variance. Figure 10 presents the Lagrangian dispersion function [corresponding to Eq. (6)] in a similar fashion as shown in the other figures (Figs. 8 and 9). It is somewhat difficult to interpret the patterns of behavior of the dispersion function in the light of existing statistical theories, as most of these theories have been developed for very specific regimes such as decaying turbulent flows (Basdevant and Sadourney 1983; McWilliams 1984) and forced turbulent regimes (Basdevant et al. 1981). For inhomogeneous turbulent regimes, as considered here, the theoretical relations determining the time evolution of the Lagrangian statistics are not able to predict the actual behavior.

The inhomogeneity of the turbulent velocity field is superimposed on a shear of the velocity field. This characteristic of the mean velocity field also needs to be taken into consideration when estimating Lagrangian statistics.

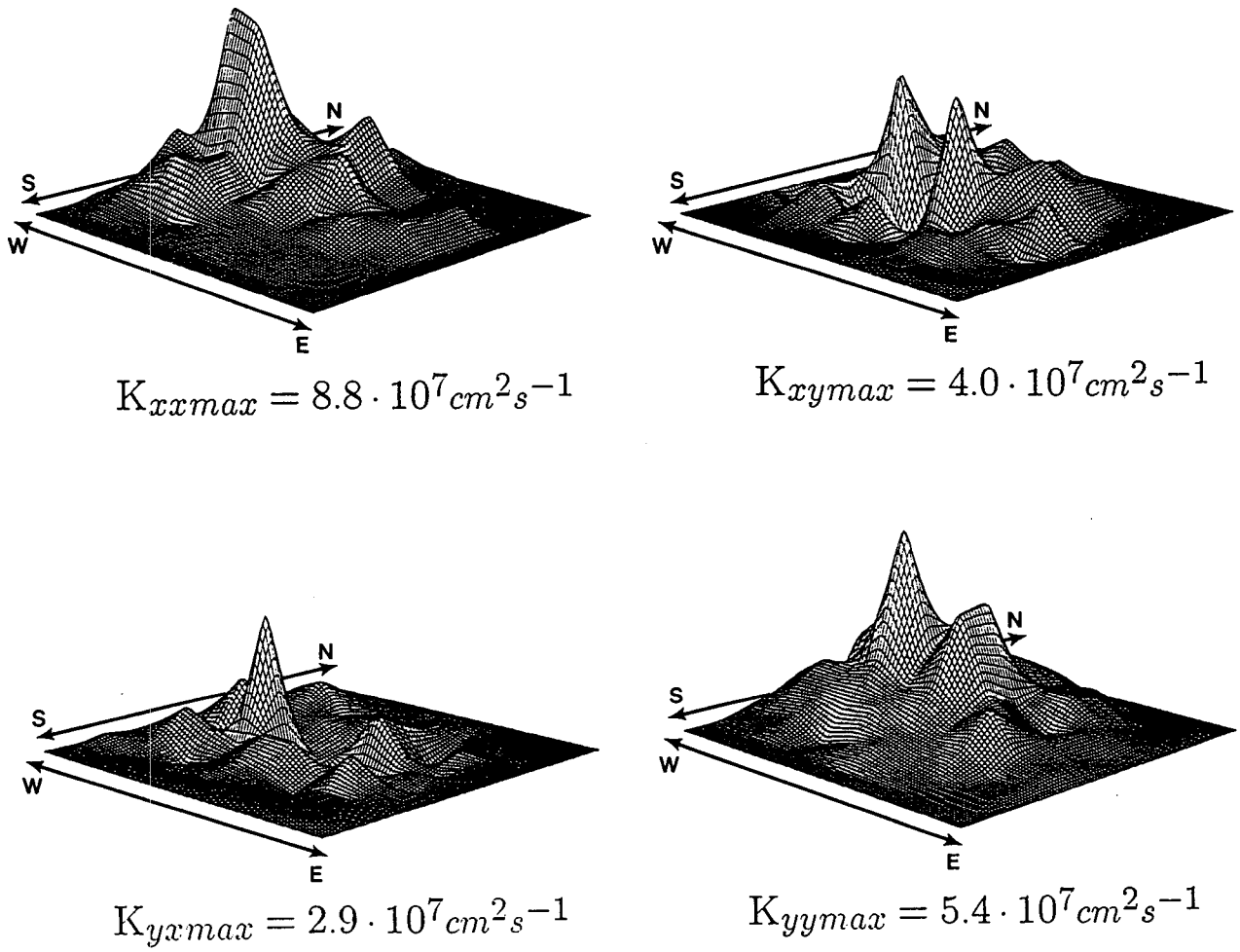

FIG. 9. Map of the four elements of the isopycnal diffusivity matrix.

The relation between Lagrangian velocity statistics and simple shear flows was first analyzed by Corrsin (1953) by considering a statistically homogeneous and stationary Eulerian velocity field with a linear shear. The expression for the dispersion tensor element on the direction across the shear as $t \to \infty$ suggests a t^3 growth law rather than the t^2 characteristic of no shear flows. This t^3 law is more likely to explain the Lagrangian dispersion better than the t^2. It should be noted, however, that a t^3 growth law only considers the mathematical aspect of the derivation of the growth rate and does not take into account the direct influence of the shear on the dispersion of the particles. That is, particles in a region of strong shear can be actually inhibited from dispersing across the shear flow. This effect, which suggests a strong interaction between the trajectory of the particles and strong jets, cannot be removed in any simple manner.

b. The deformation-dependent diffusivity field

A variable eddy diffusivity described as "deformation dependent" (Smagorinsky 1963), which provides for large eddy diffusion in regions where the horizontal shear of the velocity field is large, is estimated from the Eulerian velocity field. The space-dependent deformation diffusivity [Eq. (7)] is computed by averaging in time the instantaneous velocity shear from the eddy resolving model. This leads to an isotropic and inhomogeneous diffusivity coefficient defined as

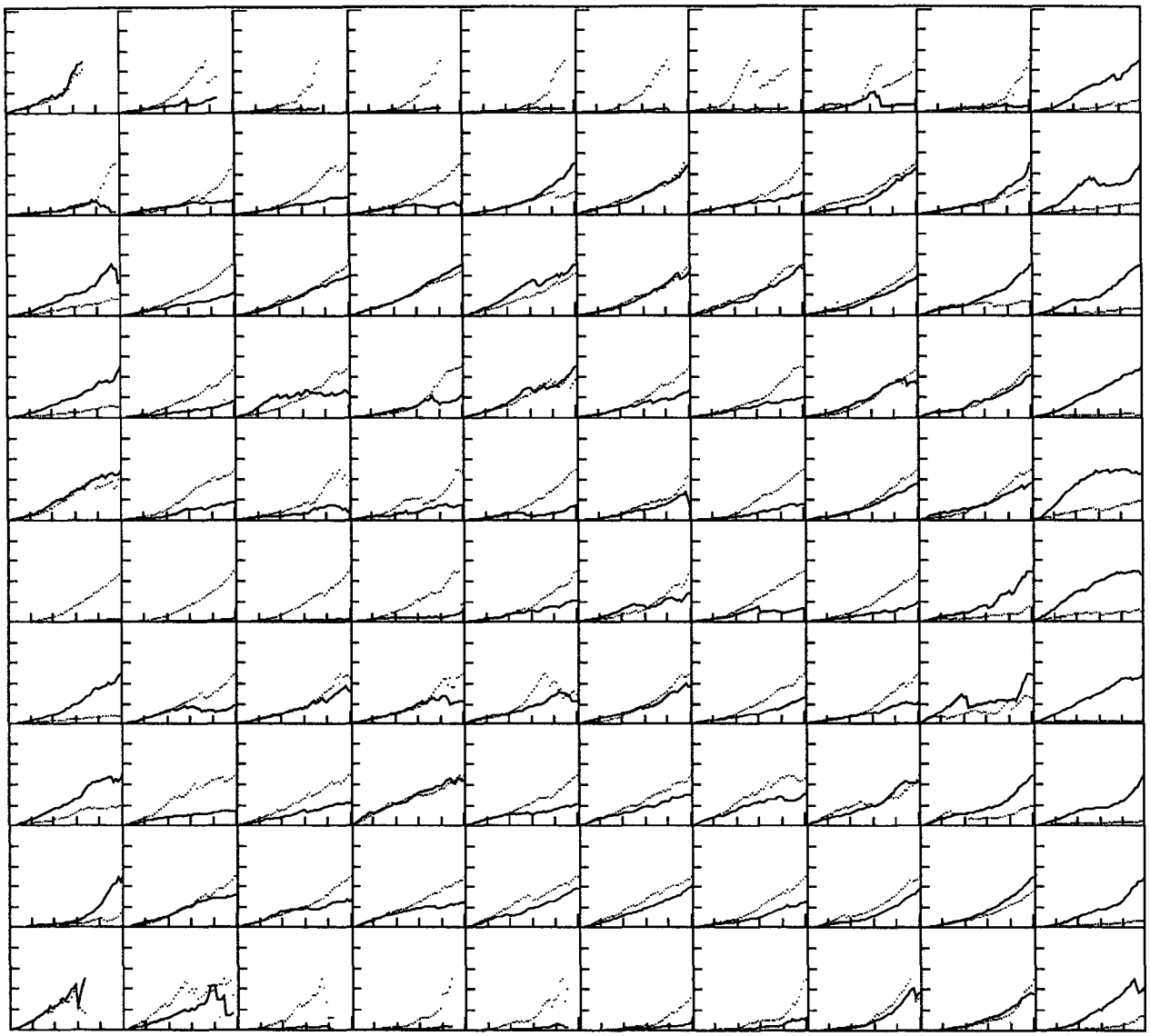

FIG. 10. Map of the dispersion function estimated according to Eq. (6). The x axis in each frame corresponds to a time lag that goes from 0 to 30 days. The y axis varies for each frame.

$$K_H(x, y) = \frac{\alpha \Delta x \Delta y}{T} \times \int_0^T \left[\overbrace{\left(\frac{\partial u}{\partial x} - \frac{\partial v}{\partial y} \right)^2}^{N} + \overbrace{\left(\frac{\partial v}{\partial x} + \frac{\partial u}{\partial y} \right)^2}^{S} \right]^{1/2} dt. \quad (7)$$

The proportionality constant α, chosen such that the basin-averaged diffusivity coefficient is approximately the same as in the other experiments (10^7 cm^2 s^{-1}) is equal to 0.6. The spatial velocity gradients are computed at regular time intervals from the eddy-resolving model and averaged in time to obtain the mean shear (S) and normal (N) stresses. The spatial distribution of the deformation-dependent diffusivity is presented in Fig. 11. The reasoning behind the use of the deformation-dependent diffusivity is interpreted as follows: the formation and maintenance of the eddy field requires an energy source, which is mostly provided by the shear flow. Thus, the magnitude of the shear gives a measure of the intensity of the eddy field that it sustains. This relationship can be expressed as

$$\frac{u'}{l} = c \frac{\partial u_i}{\partial x_j},$$

where c is a nondimensional constant. If c is order 1, the vorticity of the eddies is of the same scale as the

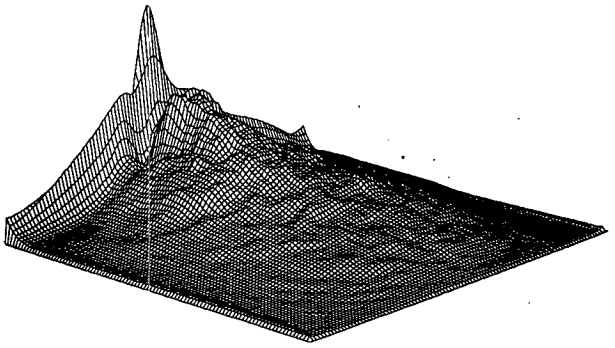

FIG. 11. Deformation-dependent diffusivity. Maximum value is 5.7×10^7 cm^2 s^{-1}.

mean shear. If a mixing length model is invoked, where $K \sim u'l$ or $K \sim u'^2 T$, we can further write

$$K \sim cl^2 \frac{\partial u_i}{\partial x_j} \sim c^2 l^2 \left(\frac{\partial u_i}{\partial x_j}\right)^2 T,$$

where i and j represent the two horizontal directions. The first form of these two expressions is assumed here. The modulus in Eq. (7) guarantees a nonnegative diffusivity field. Therefore, the use of the deformation-dependent diffusivity is consistent with mixing length theories. Its geographical distribution is thus qualitatively similar to the combination of the diagonal terms of the Lagrangian diffusivity field.

5. Conclusions

From the trajectories of 200 particles released in an eddy resolving numerical model, a Lagrangian description of the model ocean circulation is presented. This description is based on the analysis of individual trajectories as well as on the estimation of Eulerian and Lagrangian statistics.

The Lagrangian trajectories presented here, show many of the features observed from floats in the real ocean: some of them are trapped in eddies and drift with them for several months before escaping; others shows the effect of propagating waves. However, almost no particles are observed to cross from one gyre to the other through the meandering jet, although some do so farther downstream.

By using a combination of Lagrangian and Eulerian statistics, it is observed that with a large number of particles the mean Eulerian velocities and velocity variances can be estimated well from the Lagrangian trajectories. However, the estimation of Lagrangian statistics in this study, particularly near the western boundary layer, is not significantly dependent on the sample size but rather on the ratio of the local advective time scale to the Lagrangian decorrelation time scale. That is, if the mean flow is too fast for the Lagrangian particle to stay inside the bin for time longer than its decorrelation time, the K^∞ is never reached. This cannot be improved by increasing the number of particles used to estimate the diffusivity function.

The estimation of the spatial distribution of the diffusivity function from the trajectories of the particles released in the eddy-resolving numerical model depict most of the characteristics observed from oceanic estimations: 1) anisotropy of the horizontal components of the diffusivity matrix with zonal values usually being larger than meridional diffusivities, and 2) an inhomogeneous diffusivity field, with large values in those regions where the eddy kinetic energy is larger. It also shows that the off-diagonal elements of the diffusivity matrix are of the same order of magnitude as the diagonal elements. On the other hand, these Lagrangian statistical estimates from the numerical simulations also proved to have some of the same computational complications as the oceanic estimations, particularly in those areas of strong velocities (e.g., western boundary currents). One of the major limitations of estimating diffusivities from Lagrangian trajectories is that when the Eulerian advective time scale is smaller than the decorrelation time of the Lagrangian trajectory, the diffusivity function does not reach an asymptotic value as expected from theory. This characteristic of the diffusivity function in high velocity regions is intrinsic to the closure approximation. This troubling aspect of the Lagrangian sampling problem is particularly critical when trying to quantitatively describe the typical features of the general circulation using Lagrangian statistics. This is a manifestation of the inhomogeneity and nonstationarity of the velocity field. Unfortunately, these characteristics are stronger in those regions where Lagrangian diffusivity estimates are believed to be more important (e.g., western boundary currents) and weaker in those regions where knowledge of their numerical values is less relevant. The model diffusivity coefficients were consistent in magnitude and spatial distributions with oceanic estimates: higher values in western boundary currents and their seaward extensions, higher zonal than meridional values over most of the basin, and lower diffusivity values in the ocean interior. These two last statements suggest that, in principle, there is no need for an extremely large number of drifters to map the diffusivity field in the ocean, because the basic characteristics probably can be estimated with a few drifters, while the more involved properties (e.g., the diffusivity function) cannot be estimated even if the number of floats is increased significantly.

Consistent with mixing length theories, the deformation-dependent diffusivity spatial distribution is very similar to the Lagrangian diffusivity, although the former has large values near the western boundary layers.

The preceding statements regarding the representativeness of the results compared to oceanic estimates contain good news and bad news. The good news is that the results are in agreement with what is known about the eddy diffusivity field in the ocean, giving some credibility to the conclusion. The bad news is that the results suggest that the consistency of some statistics computed here cannot be improved by increasing the sample size. This is of particular relevance for field program implementation plans, as it sets limits on the attainable spatial resolution of the diffusivity field in the ocean.

The major question left to answer is how useful these diffusivity fields are for describing the evolution in time of a passive tracer field. This answer is the topic of Part II.

Acknowledgments. Discussions with Annalisa Griffa, Michael Brown, and Peter Rhines were most helpful. This work was supported by the following grants from the Office of Naval Research: to Dr. Otis Brown under Contracts N00014-85-C0020, N00014-87-K0008 and to Dr. Donald Olson under Contracts N00014-87-G0116, N00014-89-J1137, and N00014-90J-1476. Support from these grants is gratefully acknowledged.

APPENDIX

The Particle Tracking Problem

The Lagrangian representation of the velocity field depends primarily on the accuracy of the interpolation scheme used to calculate the fluid particle velocity at the particle's exact position and the temporal resolution of the velocity field, or size of time step. Another source of error arises from the fact that there is always some part of the energy spectra of motion that is not being resolved, and its interaction with the resolved field is unknown. This source of error was analyzed to some extent by Haidvogel (1982).

a. The interpolation scheme

Three different two-dimensional interpolation schemes were tested to find the one that produces the smallest positioning error. These are the bicubic interpolation scheme, bicubic spline, and polynomial interpolation scheme. These three schemes are discussed in Press et al. (1986). The performance of each of these schemes was analyzed by estimating the least error for a given analytical field. The maximum error (not shown here) associated with the polynomial interpolation scheme is one order of magnitude smaller than that of the bicubic spline. As expected, in regions where the gradient of the function is larger the error in the interpolation is larger. The root-mean-square error for the polynomial scheme is less than 0.5% of the value of the function. Yeung and Pope (1988) find that cubic splines gives the higher interpolation accuracy from a comparison of ten different interpolation schemes. In that paper, however, the polynomial interpolation scheme used in this study is not considered, and interpolations are performed in three dimensions rather than two, as is the case here.

b. The Lagrangian scheme

The path of a particle is determined by the kinematic requirement that

$$\frac{d\mathbf{x}(t)}{dt} = \mathbf{u}(\mathbf{x}(t), t), \tag{8}$$

where $\mathbf{u}$ is the horizontal velocity field, which is a function of the position $\mathbf{x}$ and time t. The simplest form of integration is usually referred to as the Euler or kinematic method and consists of obtaining the particle position at a new time step, based on the velocity at the position of the present time step. This can be written as

$$x_i^{n+1} = x_i^n + \Delta T[u(x, t^n)], \tag{9}$$

where the superscripts indicate the time level and $\Delta T = t^{n+1} - t^n$. The trajectories are given by a vector equal to the displacement between the points (x^n, y^n) and (x^{n+1}, y^{n+1}).

The assessment of the accuracy of the trajectories of particles embedded in a given velocity field was approached by considering two different types of velocity fields and two different Lagrangian schemes. The former are a time-independent analytical velocity field and the velocity field arising from the primitive equation model of Bleck and Boudra (1986), and the latter are a fourth-order Runge–Kutta and the Euler scheme. Although the results from this comparison are not shown here, it was observed that for the velocities and small time steps used in the integration of the model the Euler scheme performs as well as a fourth-order Runge–Kutta scheme. Note that the fourth-order Runge–Kutta scheme requires knowledge of the velocity components at four successive times (and positions) per time step. These positions (and corresponding velocities) correspond to the positions (and velocities) where the particle is going to be at future times. Thus, the use of a higher-order scheme for velocity fields defined at grid points does not necessarily imply an increase in accuracy for sufficiently small steps, such as used here.

REFERENCES

Basdevant, C., and R. Sadourney, 1983: Modelisation des echelles virtuelles dans la simulation numerique des ecoulements turbulents bidimensionnels. *J. Mec. Theor. Appl.*, (Numero Special), 243–270.

——, B. Legras, R. Sadourney, and M. Beland, 1981: A study of barotropic model flows: Intermittency waves and predictability. *J. Atmos. Sci.*, **38**, 2305–2326.

Bleck, R., 1978: Finite difference equations in generalized vertical coordinates. Part I: Total energy conservation. *Contrib. Atmos. Phys.*, **51**, 360–372.

——, and D. B. Boudra, 1981: Initial testing of a numerical ocean circulation model using a hybrid (quasi-isopycnic) vertical coordinate. *J. Phys. Oceanogr.*, **11,** 755–770.

——, and ——, 1986: Wind-driven spin-up in eddy-resolving ocean models formulated in isopycnic and isobaric coordinates. *J. Geophys. Res.*, **91c,** 7611–7621.

Böning, C. W., and M. D. Cox, 1988: Particle dispersion and mixing of conservative properties in an eddy-resolving model. *J. Phys. Oceanogr.*, **18,** 320–338.

Boudra, D., and E. Chassignet, 1988: Dynamics of Agulhas Retroflection and Ring Formation in a Numerical Model. Part I: The vorticity balance. *J. Phys. Oceanogr.*, **18,** 281–303.

Bower, A. S., 1991: A simple kinematic mechanism for mixing fluid parcels across a meandering jet. *J. Phys. Oceanogr.*, **21,** 173–180.

——, and T. H. Rossby, 1989: Evidence of cross-frontal exchange processes in the Gulf Stream based on isopycnal RAFOS float data. *J. Phys. Oceanogr.*, **19,** 1177–1190.

Campos, E., and D. B. Olson, 1991: Stationary Rossby waves in western boundary current extensions. *J. Phys. Oceanogr.*, **21,** 1202–1224.

Colin de Verdiere, A., 1983: Lagrangian eddy statistics from surface drifters in the eastern North Atlantic. *J. Mar. Res.*, **41,** 375–398.

Corrsin, S., 1953: Remarks on turbulent heat transfer. *Proc. of the Iowa Thermodynamics Symp.*, Iowa City, University of Iowa, 5–30.

Davis, R. E., 1983: Oceanic property transport, Lagrangian particle statistics, and their prediction. *J. Mar. Res.*, **41,** 163–194.

——, 1985: Drifter observations of coastal surface currents during CODE: The statistical and dynamical views. *J. Geophys. Res.*, **90**(C3), 4756–4772.

——, 1987: Modeling eddy transport of passive tracers. *J. Mar. Res.*, **45,** 635–666.

——, 1991: Lagrangian ocean studies. *Ann. Rev. Fluid Mech.*, **23,** 43–64.

Dewar, W. K., and G. R. Flierl, 1985: Particle trajectories and simple models of transport in coherent vortices. *Dyn. Atmos. Oceans,* **9,** 215–252.

Figueroa, H. A., and D. B. Olson, 1989: Lagrangian statistics in the South Atlantic as derived from the SOS and FGGE drifters. *J. Mar. Res.*, **47,** 525–546.

Freeland, H. J., P. Rhines, and H. T. Rossby, 1975: Statistical observations of trajectories of neutrally buoyant floats in the North Atlantic. *J. Mar. Res.*, **33,** 383–404.

Haidvogel, D. B., 1982, On the feasibility of particle tracking in Eulerian ocean models. *Ocean Modelling* (Unpublished manuscript), **45,** 4–9.

Holland, W. R., 1978: The role of mesoscale eddies in the general circulation of the ocean-numerical experiments using a wind-driven quasi-geostrophic model. *J. Phys. Oceanogr.*, **8,** 363–392.

——, and L. B. Lin, 1975: On the generation of mesoscale eddies and their contribution to the oceanic general circulation. *J. Phys. Oceanogr.*, **5,** 642–657.

Huang, R. X., 1986: Numerical simulation of wind-driven circulation in a subtropical subpolar basin. *J. Phys. Oceanogr.*, **16,** 1636–1650.

Kao, S. K., 1965: Some aspects of the large-scale turbulence and diffusion in the atmosphere. *Quart. J. Roy. Meteor. Soc.*, **91,** 10–17.

Krauss, W., and C. W. Böning, 1987: Lagrangian properties of eddy fields in the northern North Atlantic as deduced from satellite-tracked buoys. *J. Mar. Res.*, **45,** 259–291.

McWilliams, J. C., 1984: The emergence of isolated coherent vortices in turbulent flow. *J. Fluid Mech.*, **146,** 21–43.

Owens, W. B., 1984: A synoptic and statistical description of the Gulf Stream and subtropical gyre using SOFAR floats. *J. Phys. Oceanogr.*, **14,** 104–113.

Piola, A. R., H. A. Figueroa, and A. Bianchi, 1987: Some aspects of the surface circulation south of 20°S from the FGGE drifters. *J. Geophys. Res.*, **92,** 5101–5114.

Press, W. H., B. P. Flannery, S. A. Tenkolsky, and W. T. Vetterling, 1986: *Numerical Recipes.* Cambridge Press, 818 pp.

Richardson, P. L., 1983: Eddy kinetic energy in the North Atlantic from surface drifters. *J. Geophys. Res.*, **88**(C7), 4355–4367.

Smagorinsky, J. S., 1963: General circulation experiments with the primitive equations. Part I: The basic experiment. *Mon. Wea. Rev.*, **91,** 99–164.

Taylor, G. I., 1921: Diffusion by continuous movements. *Proc. London Math. Soc.*, **20,** 196–212.

Yeung, P. K., and S. B. Pope, 1988: An algorithm for tracking fluid particles in numerical simulations of homogeneous turbulence. *J. Comput. Phys.*, **79,** 373–416.

Zalezak, S. T., 1979: Fully multidimensional flux-corrected transport algorithms for fluids. *J. Comput. Phys.*, **31,** 335–362.